HHS Public Access

Author manuscript

Metab Eng. Author manuscript; available in PMC 2020 July 01.

Published in final edited form as:

Metab Eng. 2019 July ; 54: 286–291. doi:10.1016/j.ymben.2019.04.011.

A Designed Bacterial Microcompartment Shell with Tunable Composition and Precision Cargo Loading

Bryan Ferlez[a,b], **Markus Sutter**[a,b,c], **Cheryl A. Kerfeld**[a,b,c,*]

[a]MSU-DOE Plant Research Laboratory, Michigan State University, 612 Wilson Road, East Lansing, MI 48824, USA

[b]Department of Biochemistry and Molecular Biology, Michigan State University, 603 Wilson Road, East Lansing, MI 48824, USA

[c]Environmental Genomics and Systems Biology and Molecular Biophysics and Integrated Bioimaging Divisions, Lawrence Berkeley National Laboratory, 1 Cyclotron Road, Berkeley, CA 94720, USA

Abstract

Microbes often augment their metabolism by conditionally constructing proteinaceous organelles, known as bacterial microcompartments (BMCs), that encapsulate enzymes to degrade organic compounds or assimilate CO_2. BMCs self-assemble and are spatially delimited by a semi-permeable shell made up of hexameric, trimeric, and pentameric shell proteins. Bioengineers aim to recapitulate the organization and efficiency of these complex biological architectures by redesigning the shell to incorporate non-native enzymes from biotechnologically relevant pathways. To meet this challenge, a diverse set of synthetic biology tools are required, including methods to manipulate the properties of the shell as well as target and organize cargo encapsulation. We designed and determined the crystal structure of a synthetic shell protein building block with an inverted sidedness of its N- and C-terminal residues relative to its natural counterpart; the inversion targets genetically fused protein cargo to the lumen of the shell. Moreover, the titer of fluorescent protein cargo encapsulated using this strategy is controllable using an inducible tetracycline promoter. These results expand the available set of building blocks for precision engineering of BMC-based nanoreactors and are compatible with orthogonal methods which will facilitate the installation and organization of multi-enzyme pathways.

Keywords

bacterial microcompartments; protein design; metabolic engineering; synthetic biology

1. Introduction

Many bacteria compartmentalize segments of their metabolism within self-assembling proteinaceous nanoscale structures known as bacterial microcompartments (BMCs).[1,2] A semi-permeable polyhedral shell composed of cyclic hexamers (BMC-H), pseudohexameric

*Corresponding author ckerfeld@lbl.gov.

trimers (BMC-T), and pentamers (BMC-P), serves as both a scaffold to organize encapsulated enzymes as well as a physical boundary to reduce diffusive loss of volatile or toxic intermediates and restrict crosstalk with cytosolic pathways.[3–5] BMCs carry out a range of different metabolic reactions, including carbon fixation and the degradation of small carbon compounds (e.g. choline, 1,2-propanediol, ethanolamine). Many of the enzymes central to these anabolic and catabolic pathways are targeted to the BMC lumen via encapsulation peptides (EP_S), typically located at their N- or C- termini, that interact non-covalently with the luminal surface of the shell.[6–9] However, formation of BMC shells is not dependent on the presence of EP-possessing enzymes; empty intact shells can assemble in the absence of native cargo when BMC-H, BMC-T, and BMC-P proteins are either expressed heterologously,[10–12] or combined in vitro.[13] The ability to construct empty shells provides the possibility to target non-native enzymes and ultimately construct new subcellular nanoreactors to augment the metabolism of a bacterial host.

Unfortunately, repurposing EPs from BMC-associated enzymes has been only modestly successful in directing non-native cargo to the lumen of heterologous shells, in part due to the propensity for EPs to promote aggregation.[14,15] An alternative strategy is the translational fusion of cargo directly to individual shell proteins. However, this approach requires both knowledge and control of the sidedness and composition of the BMC shell in order to facilitate cargo placement and loading titers. For example, in the recent atomic-level crystal structure of the empty 6.5 MDa BMC shell from *Haliangium ochraceum* (HO shell), the N-and C-termini of most shell proteins are located on the outside of the shell;[16] translational fusion of protein cargo to the termini of any of these building blocks would lead to display on the outer surface rather than encapsulation within the BMC lumen. Furthermore, as in other BMC shells,[17] BMC-H are the numerically dominant component of the HO shell and provide an attractive target for maximizing the number and/or distribution of encapsulated proteins if fusions with the individual BMC-H protomers could be directed toward the lumen.[16] Here we designed and report the structure of a circularly permuted version of the BMC-H protein (CPH) from the HO shell that oligomerizes into hexamers and has new N- and C-termini, relocated to its luminal face. CPH, along with BMC-T and BMC-P, assemble into shells similar in size and morphology to the unmodified HO shell. GFP fused to the C-terminus of CPH incorporates into the shell, is localized to the lumen, and its titer can be controlled using an inducible tetracycline promoter. Our rationally designed circularly permuted building block provides precise control over sidedness and quantitative cargo incorporation for the construction of new BMC nanoreactors.

2. Results and Discussion

2.1 Design and structure of a circularly permuted shell protein that assembles into shells

All BMC-H proteins contain a single BMC domain (pfam 00936) that consists of three alpha-helices, four beta-strands, and is ~100 amino acids in length.[18] Cyclic hexamers of BMC-H proteins form discoids; hexagons approximately 7 nm across and 2 nm thick with a distinct convex and concave face. The N- and C-termini of the wild type BMC-H (WTH) from the HO shell are located on the concave side of the hexamer and therefore on the outer surface of the shell.[16] The ~10 C-terminal residues of WTH appear to lack any secondary

structure and, in the crystal structure (pdb 5djb), the distance between the N- and C-termini is only ~13 Å.[19] The potential flexibility of the C-terminal residues and the spatial proximity of the N- and C-termini suggest WTH is amenable to circular permutation, a rearrangement of secondary structure elements that, in this case, serves the purpose of creating new N- and C-termini on the luminal face of the hexamer. To circularly permute the WTH protein, its primary structure is first separated into two parts: residues Ala2-Gly68 (beta-strand 1 to alpha-helix 2) (Figure 1a, blue) and residues Glu69-Ala99 (beta-strand 4 to alpha-helix 3) (Figure 1a, green). Moving the latter segment to the start of the polypeptide and joining the original N- and C-termini (between alpha-helix 3 and beta-strand 1) with a flexible $(Gly\text{-}Ser)_3$ linker introduces new N- and C-termini in a short loop region located on the convex side which faces the inside when incorporated in a shell (Figure 1a). The 1.6 Å x-ray crystal structure of the individual CPH protomer (pdb 6nlu, Table S1) has a rmsd of 0.2 Å when superimposed onto the alpha carbons of the unpermuted WTH structure (pdb 5djb); no electron density was observed for the majority of the $(Gly\text{-}Ser)_3$ linker, indicating that it is flexible (Figure 1b). Moreover, CPH forms a cyclic hexamer like WTH (Figure 1c), suggesting it could assemble into shells with luminal-facing N- and C-termini if expressed in the presence of BMC-T and BMC-P proteins (Figure 1d). To test if CPH can substitute for WTH in the context of the HO shell, CPH shells were isolated using the rapid complementary affinity-based purification (CAP) technique recently developed for HO shells consisting of BMC-H (WTH), BMC-T_1(T_1) and strep-II-tagged BMC-P (P_{SII}).[20] When CPH, T_1, and P_{SII} are co-expressed in *E. coli,* negative-stained transmission electron microscopy (TEM) shows intact shells with similar morphology and size ($d = 37 \pm 3$ nm, $n = 245$) to the shell with the unpermuted BMC-H can be purified from the cell lysate using CAP (Figure 1e), indicating that CPH can structurally substitute for WTH.

In contrast, two reports of the circular permutation of PduA (CP-PduA), one of the predominant BMC-H proteins in the propanediol utilization (PDU) BMC,[17] had different structural and morphological outcomes despite using similar designs. In one report, the crystal structure of CP-PduA revealed a pentameric rather than hexameric oligomeric state that assembles into small (d ~ 13 nm) nanocages in the absence of other shell proteins.[21] In the second study, although no direct measurement of the oligomeric state was reported, CP-PduA was able to incorporate into PDU shells in *E. coli,* and when expressed alone, formed extended structures consistent with a hexameric state. However, because CP-PduA (or PduA) is not required for the formation of heterologous PDU shells due the presence of additional BMC-H homologs (i.e. PduJ, PduK, PduU), the final number of incorporated CP-PduA proteins remain unclear. Moreover, the incorporation of CP-PduA into PDU shells prevented their purification using standard protocols used for isolation of PDU shells.[22]

2.2 Incorporation of genetically fused cargo into CPH shells

The ability to assemble and purify CPH-T_1-P_{SII} shells from *E. coli* enables screening for successful incorporation of genetically fused cargo by SDS-PAGE, western blot, and TEM analyses. As a proof-of-principle, a C-terminal hexahistidine (his6) tagged superfolder GFP[23] (GFP) fused to the C-terminus of CPH (CPH-GFP_{his6}) was co-expressed with a CPH_{his6}-T_1- P_{SII} shell (a hexahistidine tag was appended to the C-terminus of CPH (CPH_{his6}) to enable western blot detection). Retaining a copy of CPH_{his6} and regulating

expression of CPH-GFP_{his6} from a separate plasmid prevents steric clashes that would arise from too many GFP molecules on the shell lumen; indeed, when only CPH-GFP_{his6} is co-expressed with T_1 and P_{SII}, no shells are formed (data not shown). The presence of a ~40 kDa band on SDS-PAGE of purified CPH_{his6}-T_1-P_{SII} /CPH-GFP_{his6} shells provides support for the incorporation of CPH-GFP_{his6} (~38.4 kDa) (Figure 2a) and is further substantiated by the visibly green color of the sample. The presence of CPH-GFP_{his6} as well as CPH_{his6} and P_{SII} are confirmed by western blotting using anti-his (Figure 2b) and anti-Strep (Figure 2c) antibodies. TEM analysis of this sample confirms the presence of shells with a diameter of 40 ± 3 nm (n = 130) (Figure 2d). In addition, a higher magnification view of the TEM micrograph of shells shows a thicker shell wall (Figure 2e) when compared to a similarly magnified view of the CPH-T_1- P_{SII}-shells shown in Figure 1e (Figure 2f). A thicker shell is consistent with the presence of GFP_{his6} fused to some of the CPH. While it is possible that staining differences during TEM sample preparation could account for this increased shell thickness, similar morphological differences have previously been observed when fluorescent proteins are targeted to the lumen of the HO shell by covalent attachment to T_1, [20] or non-covalent attachment to WTH.[13]

2.3 GFP cargo is targeted to the luminal face of intact CPH shells

To confirm the orientation of the C-terminus of CPH, we probed the susceptibility of the C-terminal his-tags of CPH-GFP_{his6} as well as CPH_{his6} to proteolysis by bovine carboxypeptidase A (CPA). CPA catalyzes the removal of a broad range of C-terminal aromatic and aliphatic residues, including histidine.[24,25] The sidedness of the C-terminal his-tags can therefore be tracked by monitoring the anti-his detected western blot signals from samples following exposure to CPA. C-terminal his-tags located within the shell's lumen are protected from proteolysis because the ~35 kDa CPA enzyme is too large to pass through the central pores of hexamer, trimer, or pentamer shell subunits; while a surface exposed his-tag is susceptible to proteolysis (Figure 3a). Throughout 120 minutes of CPA exposure, the majority of the anti-his western blot signals from both CPH_{his6} and CPH-GFP_{his6} appear to be retained, suggesting protection from proteolysis (Figure 3b, top). CPH_{his6}-T_1-P_{SII} shells incorporating WTH-GFP_{his6} (Figure S2), which has an outward facing C-terminal his-tag, were used as a control. The western blot signal for WTH-GFP_{his6} incorporated into CPH_{his6}-T_1-P_{sII} shells was almost completely lost after 30 minutes of exposure to CPA while the CPHhis6 signal remained relatively unchanged throughout the time course (Figure 3b, bottom). Interestingly, the WTH-GFP_{his6} anti-his western blot signal is not completely lost even after 120 minutes of exposure to CPA. This fraction of WTH-GFP_{his6} may represent a small population either stochastically encapsulated within the lumen or with sterically occluded C-termini due to their position on the surface of the shell. These results confirm that the we successfully generated a BMC-H that localizes translationally fused cargo on the luminal side of intact BMC shells.

2.4 Control and quantification of the number of encapsulated GFP molecules

An advantage of engineering BMC-H proteins is that they constitute the majority of the surface, or potential scaffolding, of the shell; HO shells consist of 60 hexamers, 20 trimers and 12 pentamers.[16] Using our two-plasmid expression system we determined the maximum loading capacity of GFP molecules per hexamer and shell by titrating the

induction level of CPH-GFP_{his6} with anhydrotetracycline (aTc) while supplying a constant amount of IPTG to induce the CPH_{his6}-T_1-P_{SII} shell components. Absorption spectra of shells purified from *E. coli* cells induced with different amounts of aTc were normalized to total protein content (Figure S4) and the absorbance at 485 nm used to track relative GFP content. As the aTc concentration is raised from 0 to 25 ng Ml^{-1}, a linear ~7-fold increase in absorbance is observed indicative of increasing GFP encapsulation. When the aTc concentration is raised further to 50 ng mL^{-1}, a slight decrease in absorbance is observed suggesting that encapsulation is saturated between 25 and 50 ng mL^{-1} aTc (Figure 4a). A similar trend is also observed when the same purified shell samples are analyzed by SDS-PAGE (Figure 4b). Densitometry can be used to quantify the amount CPH-GFP_{his6} incorporated in shells by measuring the ratio of intensity between CPH-GFP_{his6} and T1 bands (assuming 20 trimers or 60 copies of T1 protein per shell). At the maximum GFP absorbance, the average ratio of CPH-GFP_{his6} to T1 is ~1.3, or ~1.3 GFP molecules per CPH hexamer and ~80 CPH-GFP_{his6} per shell (out of a total of 360 CPH chains). The length and flexibility of the linker between CPH and GFP may play an important role in determining the final titer of encapsulated cargo. In this case, the $(Gly\text{-}Ser)_3$ linker connecting CPH and GFP may be long and flexible enough to sterically preclude the incorporation of more than two fusion proteins into an individual hexamer, or, alternatively, the integration of a hexamer with more than two CPH-GFP fusions into the shell; adapting this strategy for the encapsulation of cargo larger than GFP may therefore require a smaller and/or more rigid intervening linker. Targeting cargo to the BMC lumen using CPH-fusions also has the potential to be applied in conjunction with orthogonal encapsulation methods that use T_1 as a scaffold. For example, a recently developed strategy for inserting a split adhesion domain, SpyTag or SpyCatcher,[26] within a luminal-facing loop of T_1[20] could be implemented in a CPH shell. This would allow covalent attachment of one type of cargo to T_1 using SpyTag/SpyCatcher as well as the incorporation and control over the relative titer of a second cargo directly fused to CPH. In addition, T_1 and CPH are located right next to each other, making an ideal configuration for two enzymes that catalyze sequential reactions. The combination of these strategies would extend our ability to engineer more complex BMCs by offering control not only over localization and abundance but also the relative stoichiometry of encapsulated enzymes.

2.5 Conclusions

Diversity of synthetic building blocks for construction and functionalization of BMCs is essential for realizing their metabolic potential as modular intracellular nanoreactors. Toward this goal, we designed and structurally characterized a circularly permuted BMC-H protein. CPH forms hexamers equivalent to its unpermuted form with the exception that the N- and C-termini of the individual protomers are reoriented toward the luminal face. Shells are efficiently formed in vivo by co-expressing CPH, T_1, and P_{SII} and purified similar to HO shells. In vitro protease protection assays confirm the luminal orientation of C-terminally fused GFP cargo, and by varying its induction level, the amount of CPH-GFP_{his6} protein incorporated into purified CPH_{his6}-T_1-P_{SII} shells can be titrated over a range of about 10 to 80 cargo molecules per shell. The structurally defined assembly of BMC shells with an inverted orientation of hexamer terminal residues and titratable composition. The synthetic HO shells containinshells are selectively permeable, composed of trimers and Ps too,

expands the tractable parameter space available to metabolic engineers seeking to design new subcellular compartmentalized metabolic pathways with a level of precision previously limited to containers based on a single protein such as virus-like particles[27] and lumazine synthase.[28]

3. Materials and Methods

3.1 Cloning and purification of CPH

The *E. coli* codon optimized CPH gene was synthesized (Integrated DNA technologies) and cloned into pET11b using Ndel and BamHI restriction sites (see Table S2 and S3 for a list of plasmids and amino acid sequences respectively). The resulting plasmid (pBF27) was transformed into *E. coli* BL21 (DE3) cells and induced with 0.4 mM IPTG at mid-exponential phase (OD_{600} nm = 0.6–0.8) and grown for 4 h at 37 °C. Cells were harvested by centrifugation and resuspended in buffer containing 0.05 M Tris, 0.1 M NaCl, and 0.01 M $MgCl_2$ at a density of 0.5 g Ml^{-1} and stored at −20 C until lysis. CPH was purified following the protocol for WTH from *H. ochraceum* (locus tag HO_5815) using iterative centrifugation steps and triton washes as described in the literature.[19]

3.2 X-ray Crystallography

CPH at 10.6 mg mL^{-1} (as measured by BCA) in buffer containing 0.01 M Tris pH 7.8 and 0.05 M NaCl was crystallized by vapor diffusion against a solution of 1.0 M ammonium tartrate and 0.1 M sodium acetate pH 5.1 at a protein to precipitant ratio of 2 μL:2 μL. Hexagonal crystals were looped in drop solution containing 12.5% PEG400 as a cryoprotectant after four months and frozen in liquid nitrogen. Diffraction data were collected at ALS beam line 5.0.2, integrated with XDS[29] and scaled with SCALA (CCP4).[30] Molecular replacement with phenix.phaser[31] was used with a search model of the HO-BMC- H (HO_5815, pdb 5djb) to obtain phase information. The resulting model was refined and rebuilt using phenix.refine[31] and COOT.[32] Statistics for diffraction data collection, structure determination and refinement are summarized in Table S1.

3.3 Shell expression and purification

CPH-T_1-P_{SII} (pBF36) and CPH_{his6}-T_1-P_{SII} (pBF53) shells were expressed from IPTG-inducible pETDuet-based plasmids, and when indicated, coexpressed with CPH-GFP_{his6} (pBF64) or WTH-GFP_{his6} (pBF71) from a tetracycline-inducible Bglbrick pBbA2k vector.[33] 2 L of cells were grown to mid-exponential phase (OD_{600} nm = 0.6–0.8) at 37 C in lysogeny broth supplemented with 10 μg Ml^{-1} ampicillin (for pBF53) and 50 μg mL^{-1} kanamycin (when co-transformed with pBF64 or pBF71) and induced with 0.25 mM IPTG and 0, 2, 10, 25, or 50 ng mL^{-1} aTc, briefly cold-shocked on ice for 15 min, and then grown for 20–22 h at 18 C. Cells were harvested by centrifugation and resuspended in 0.05 M Tris pH 8.0, 0.2 M NaCl to a density of 0.5 g L^{-1} and stored at −20 C until lysis. Cells were lysed by French Press at 2×10^4 psi in the presence of SigmaFast protease inhibitor (Sigma Aldrich, St. Louis USA), 0.1 mg mL^{-1} lysozyme (Sigma Aldrich, St. Louis USA), and 1 mg mL^{-1} DNase (Sigma Aldrich, St. Louis USA). Lysates were clarified by centrifugation at 27,000 × g for 30 min at 4 C. Shells were isolated from clarified lysates using CAP[20] with the addition of an initial 30% sucrose cushion (as described in Sutter et al.[16]) to remove

unincorporated P_{SII} subunits prior to applying cell lysates onto the strep column. Eluates from the strep column were further polished with a strong anion exchange column using the method described in Sutter et al.[16] Anti-his and anti-strep western blots were carried out as described for the CPA assays with the exception that the anti-strep antibody (Millipore, Burlington USA) was applied at a titer of 1:4000.

3.4 Transmission Electron Microscopy

Purified shells were imaged by negative stained TEM on a JEOL 100CXII microscope operated at an accelerating voltage of 100 kV using a Gatan Orius SC200 CCD camera. Purified shells were diluted 10-fold in HPLC-grade water and 5 μL of each sample was applied to 150 mesh carbon-coated copper grids (Electron Microscopy Sciences, Hatfield USA) for 30 s, wicked dry, stained for 15 s with 1% uranyl acetate, and again wicked dry before imaging.

3.5 Carboxypeptidase A assay

0.09 U of bovine carboxypeptidase A (Sigma Aldrich, St. Louis USA) was added per μg of total protein in a master mix of purified shells in buffer containing 0.05 M Tris pH 8.0, 0.2 M NaCl and incubated at room temperature for 120 minutes. At each time point, an equivalent volume was removed from the master mix to which SDS-PAGE sample buffer was added. The sample was immediately boiled in water for 10 min, briefly centrifuged, and placed at −20 C until samples from all time points were collected. Gels were run with equivalent volumes loaded per lane, including a T = 0 control that was prepared before the addition of CPA to the master mix; buffer (0.05 M Tris pH 8.0, 0.2 M NaCl) was added to this sample to maintain the same final concentration of protein in the SDS-PAGE sample. Following SDS-PAGE, proteins were transferred onto a nitrocellulose membrane and blocked for 4 h at room temperature with a 5% (w/v) solution of dry milk in 0.02 M Tris pH 7.8, 0.15 M NaCl, 0.3% (v/v) TWEEN 20. Membranes were incubated with HRP-conjugated anti-his antibodies at a titer of 1:3333 (Invitrogen, Carlsbad USA) for 1 h and imaged using ECL-detection reagents (General Electric, Boston USA) and a Bio-rad Chemidoc-MP imager (Bio-rad, Hercules USA). intrinsic fluorescence from GFP was recorded using the same Bio-rad Chemidoc-MP imager using the built-in GFP excitation/emission filter set to confirm equal loading between wells.

Supplementary Material

Refer to Web version on PubMed Central for supplementary material.

Acknowledgements

We would like to thank Andrew Hagen for helpful discussions and creating and sharing WT HO shell constructs that were used to generate the constructs in this paper. We also thank Aiko Turmo for help collecting preliminary TEM data and the entire Kerfeld lab for insightful discussions.

Funding

This work was supported by the Office of Science of the US Department of Energy DE-FG02–91ER20021. CAK and MS also acknowledge support from the National Institutes of Health, National Institute of Allergy and Infectious Diseases (NIAID) grant 5 R01 AI114975–05. This work used resources of the Advanced Light Source

which is supported by the Office of Science, Office of Basic Energy Sciences, of the U.S. DOE under Contract No. DE-AC02–05CH11231. The x-ray crystallographic coordinates and structure-factor files have been deposited in the Protein Data Bank (PDB) with the accession number: 6nlu.

Abbreviations

BMC	bacterial microcompartment
EP	encapsulation peptide
CP	circularly permuted
CPA	bovine carboxypeptidase-A
HO-shell	*Haliangium ochraceum* BMC shell

4. References

[1]. Axen SD, Erbilgin O, Kerfeld CA, PLoS Comput Biol 2014, 10, e1003898.

[2]. Kerfeld CA, Aussignargues C, Zarzycki J, Cai F, Sutter M, Nat Rev Microbiol 2018, 16, 277. [PubMed: 29503457]

[3]. Brinsmade SR, Paldon T, Escalante-Semerena JC, J Bacteriol 2005, 187, 8039. [PubMed: 16291677]

[4]. Sampson EM, Bobik TA, J. Bacteriol 2008, 190, 2966. [PubMed: 18296526]

[5]. Jakobson CM, Tullman-Ercek D, Slininger MF, Mangan NM, PLoS Comput. Biol 2017, 13, e1005525.

[6]. Fan C, Cheng S, Liu Y, Escobar CM, Crowley CS, Jefferson RE, Yeates TO, Bobik TA, Proc Natl Acad Sci USA 2010, 107, 7509. [PubMed: 20308536]

[7]. Fan C, Cheng S, Sinha S, Bobik TA, Proc. Natl. Acad. Sci. U.S.A 2012, 109, 14995.

[8]. Jakobson CM, Kim EY, Slininger MF, Chien A, Tullman-Ercek D, J. Biol. Chem 2015, 290, 24519.

[9]. Aussignargues C, Paasch BC, Gonzalez-Esquer R, Erbilgin O, Kerfeld CA, Commun Integr Biol 2015, 8, e1039755.

[10]. Parsons JB, Frank S, Bhella D, Liang M, Prentice MB, Mulvihill DP, Warren MJ, Molecular Cell 2010, 38, 305. [PubMed: 20417607]

[11]. Lassila JK, Bernstein SL, Kinney JN, Axen SD, Kerfeld CA, J. Mol. Biol 2014, 426, 2217. [PubMed: 24631000]

[12]. Choudhary S, Quin MB, Sanders MA, Johnson ET, Schmidt-Dannert C, PLoS ONE 2012, 7, e33342.

[13]. Hagen AR, Plegaria JS, Sloan N, Ferlez B, Aussignargues C, Burton R, Kerfeld CA, Nano Letters 2018, DOI 10.1021/acs.nanolett.8b02991.

[14]. Lee MJ, Brown IR, Juodeikis R, Frank S, Warren MJ, Metab. Eng 2016, 36, 48. [PubMed: 26969252]

[15]. Tobimatsu T, Kawata M, Toraya T, Biosci. Biotechnol. Biochem 2005, 69, 455. [PubMed: 15784971]

[16]. Sutter M, Greber B, Aussignargues C, Kerfeld CA, Science 2017, 356, 1293. [PubMed: 28642439]

[17]. Havemann GD, Bobik TA, J. Bacteriol 2003, 185, 5086. [PubMed: 12923081]

[18]. Kerfeld CA, Sawaya MR, Tanaka S, Nguyen CV, Phillips M, Beeby M, Yeates TO, Science 2005, 309, 936. [PubMed: 16081736]

[19]. Sutter M, Faulkner M, Aussignargues C, Paasch BC, Barrett S, Kerfeld CA, Liu L-N, Nano Lett. 2016, 16, 1590. [PubMed: 26617073]

[20]. Hagen A, Sutter M, Sloan N, Kerfeld CA, Nature Communications 2018, 9, 2881.

[21]. Jorda J, Leibly DJ, Thompson MC, Yeates TO, Chem. Commun. (Camb.) 2016, 52, 5041. [PubMed: 26988700]

[22]. Lee MJ, Mantell J, Brown IR, Fletcher JM, Verkade P, Pickersgill RW, Woolfson DN, Frank S, Warren MJ, Nat Commun 2018, 9, 3413. [PubMed: 30143644]

[23]. Pedelacq J-D, Cabantous S, Tran T, Terwilliger TC, Waldo GS, Nat. Biotechnol 2006, 24, 79. [PubMed: 16369541]

[24]. Gardell SJ, Craik CS, Clauser E, Goldsmith EJ, Stewart CB, Graf M, Rutter WJ, J. Biol. Chem 1988, 263, 17828. [PubMed: 3182871]

[25]. Lilius G, Persson M, Bülow L, Mosbach K, Eur. J. Biochem 1991, 198, 499. [PubMed: 1904025]

[26]. Zakeri B, Fierer JO, Celik E, Chittock EC, Schwarz-Linek U, Moy VT, Howarth M, Proc. Natl. Acad. Sci. U.S.A 2012, 109, E690. [PubMed: 22366317]

[27]. Sharma J, Uchida M, Miettinen HM, Douglas T, Nanoscale 2017, 9, 10420.

[28]. Seebeck FP, Woycechowsky KJ, Zhuang W, Rabe JP, Hilvert D, J. Am. Chem. Soc 2006, 128, 4516. [PubMed: 16594656]

[29]. Kabsch W, Acta Crystallogr D Biol Crystallogr 2010, 66, 125. [PubMed: 20124692]

[30]. Winn MD, Ballard CC, Cowtan KD, Dodson EJ, Emsley P, Evans PR, Keegan RM, Krissinel EB, Leslie AGW, McCoy A, McNicholas SJ, Murshudov GN, Pannu NS, Potterton EA, Powell HR, Read RJ, Vagin A, Wilson KS, Acta Crystallogr. D Biol. Crystallogr 2011, 67, 235. [PubMed: 21460441]

[31]. Afonine PV, Grosse-Kunstleve RW, Echols N, Headd JJ, Moriarty NW, Mustyakimov M, Terwilliger TC, Urzhumtsev A, Zwart PH, Adams PD, Acta Crystallogr. D Biol. Crystallogr 2012, 68, 352. [PubMed: 22505256]

[32]. Emsley P, Cowtan K, Acta Crystallogr. D Biol. Crystallogr 2004, 60, 2126. [PubMed: 15572765]

[33]. Lee TS, Krupa RA, Zhang F, Hajimorad M, Holtz WJ, Prasad N, Lee SK, Keasling JD, J Biol Eng 2011, 5, 12. [PubMed: 21933410]

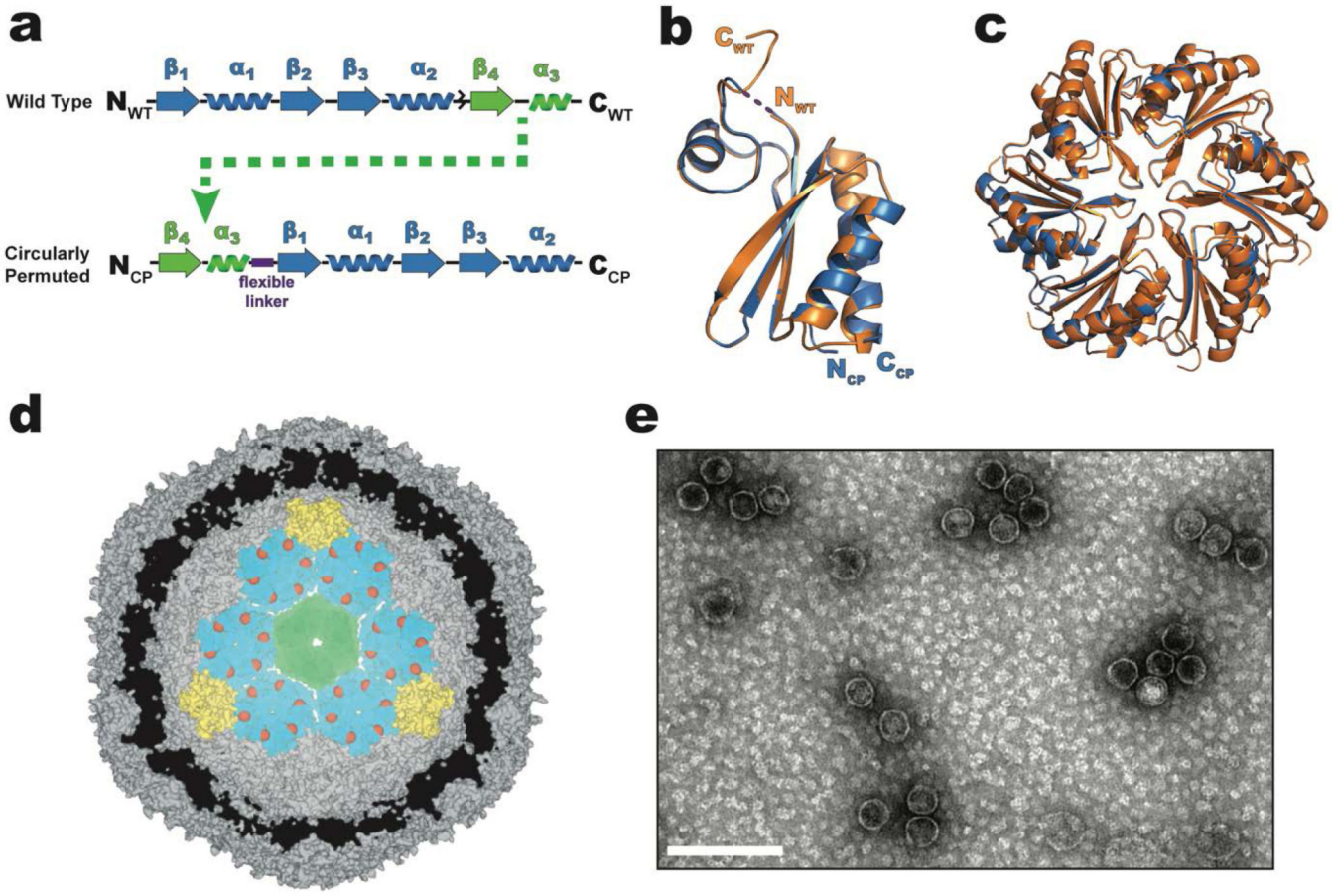

Figure 1.

Design and structure of a circularly permuted CPH protein that substitutes for the WTH in intact HO shells. a) primary structure of WTH (top) and circularly permuted CPH (bottom). The flexible $(Gly\text{-}Ser)_3$ linker used to join the original NF_{WT}- and C_{WT}- termini of WTH is represented as a purple box. b) Structural alignment of WTH (orange, pdb 5djb) and CPH (blue, pdb 6nlu) protomers. No electron density was observed for the Gly-Ser linker and is therefore drawn as a dashed line. c) Alignment of the hexameric assemblies of WTH (orange) and CPH (blue). View is top-down looking at the convex side of the hexamers. d) Cutaway model (derived from pdb 5v74) of a minimal shell made of CPH (teal), T_1 (green), and P_{SII} (yellow) proteins showing the predicted luminal orientation of the CPH C-termini (red spheres). e) TEM micrograph of purified CPH-T_1-P_{SII} shells. Scale bar is 100 nm.

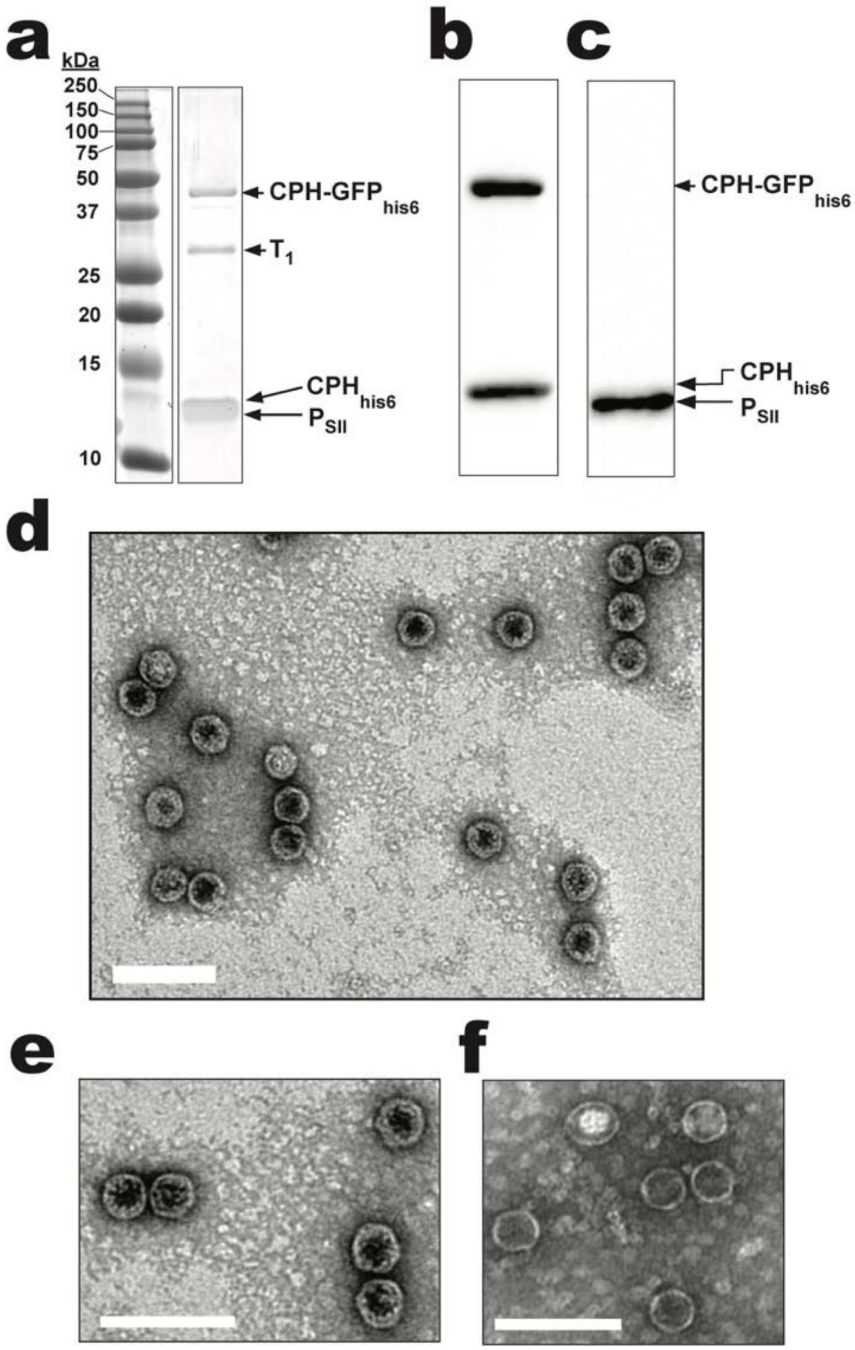

Figure 2.

CPH-GFP$_{his6}$ incorporation into CPH$_{his6}$-T$_1$-P$_{SII}$ shells. a) SDS-PAGE analysis of purified CPH$_{his6}$-T$_1$-P$_{SII}$/CPH-GFP$_{his6}$ shells (see Figure S1 for the uncropped SDS-PAGE image). b) Anti-his or c) anti-strep western blots of purified shells from (a). d) TEM micrograph of purified CPH$_{his6}$-T$_1$-P$_{sII}$/CPH-GFP$_{his6}$ shells. e) Further magnified TEM micrograph of CPH$_{his6}$-T$_1$-P$_{SII}$/CPH-GFP$_{his6}$ shells. f) For comparison, magnified TEM micrograph of CPH-T$_1$-P$_{sII}$ shells without GFP cargo from Figure 1e. Scale bars are 100 nm.

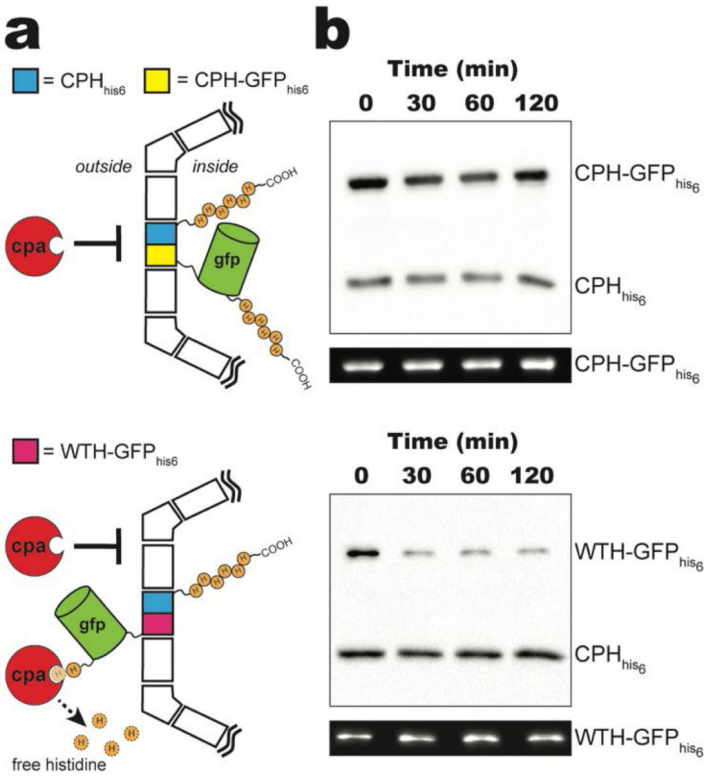

Figure 3.

In vitro protease protection assay. a) Schematic of carboxypeptidase A (CPA) protection assay for purified CPH_{his6}-T_1-P_{SII} shells incorporating CPH-GFP_{his6} (top) or WTH-GFP_{his6} (bottom). For clarity, only one CPH_{his6} (cyan) and CPH-GFP_{his6} (yellow) or WTH-GFP_{his6} (pink) is shown per shell. b) Western blot of a CPA time course of purified CPH_{his6}-T_1-P_{SII} shells incorporating CPH-GFP_{his6} (top) or WTH-GFP_{his6} (bottom) using anti-his antibodies. Representative in-blot intrinsic GFP fluorescence is shown below each western blot. See Figure S3 for uncropped fluorescence images.

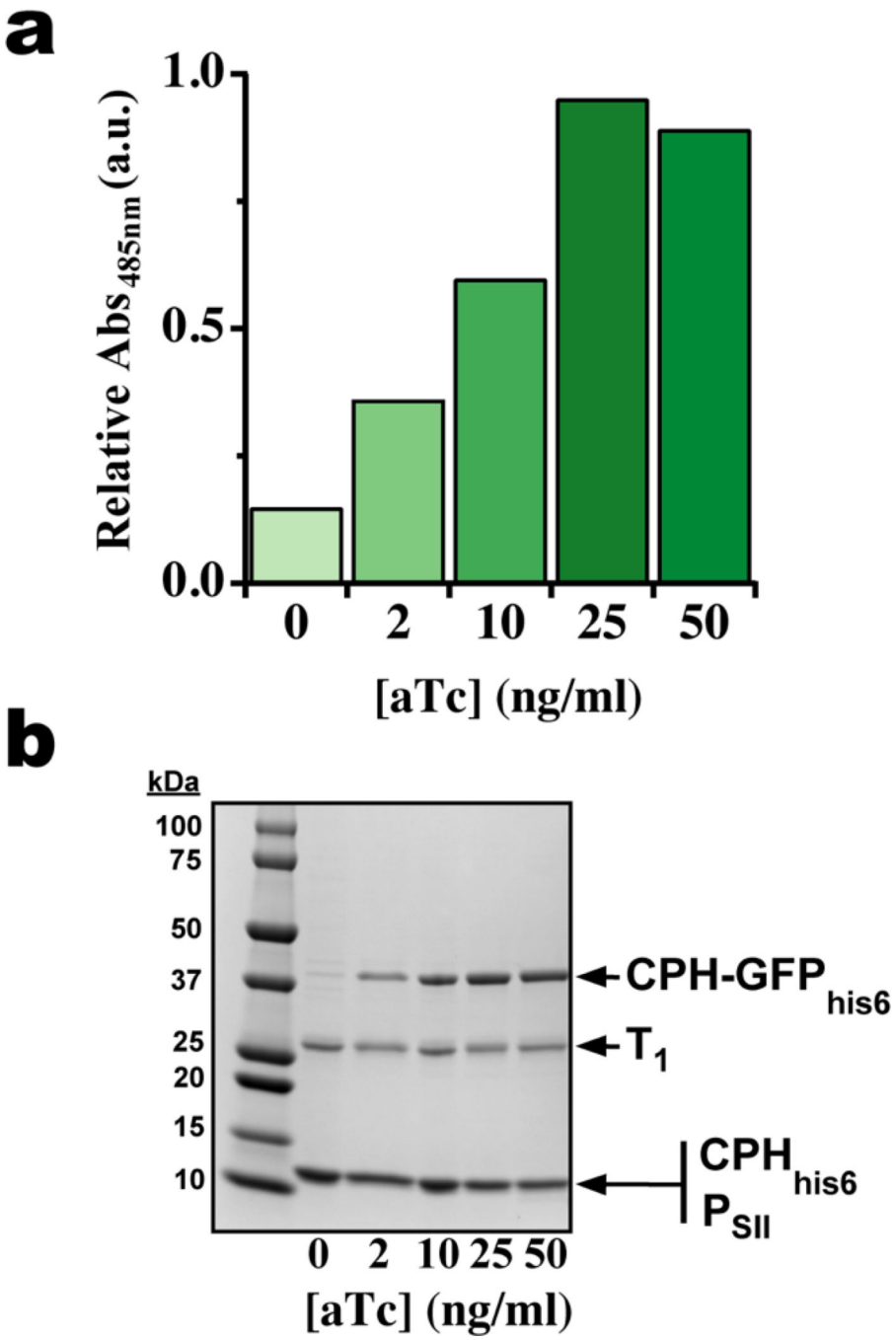

Figure 4.

CPH-GFP$_{his6}$ content of purified CPH$_{his6}$-T$_1$-P$_{SII}$ shells isolated from cells induced with different concentrations of aTc. a) GFP absorption at 485 nm from shell samples normalized by total protein content at 280 nm, a darker color indicates greater relative GFP absorbance (See Figure S4 for full spectra). b) Coomassie-stained SDS-PAGE of the same samples in (a). 2.5 μg protein loaded in each lane.